Early and Delayed STAT1-Dependent Responses Drive Local Trained Immunity of Macrophages in the Spleen

Aryeh Solomon[1], Noa Bossel Ben-Moshe[1], Dotan Hoffman[1], Sebastien Trzebanski[1], Dror Yehezkel[1], Leia Vainman[1], Mihai Netea[2,3], Roi Avraham[1]

1. Department of Immunology and Regenerative Biology, Weizmann Institute of Science, 7610001 Rehovot, Israel.
2. Department of Internal Medicine and Radboud Center for Infectious Diseases, Radboud University Medical Center, Nijmegen, Netherlands.
3. Department of Immunology and Metabolism, Life and Medical Sciences Institute, University of Bonn, Bonn, Germany.

Abstract

Trained immunity (TI) is the process wherein innate immune cells gain functional memory upon exposure to specific ligands or pathogens, leading to augmented inflammatory responses and pathogen clearance upon secondary exposure. While the differentiation of hematopoietic stem cells (HSCs) and reprogramming of bone marrow (BM) progenitors are well-established mechanisms underpinning durable TI protection, remodeling of the cellular architecture within the tissue during TI remains underexplored. Here, we study the effects of peritoneal Bacillus Calmette–Guérin (BCG) administration to find TI-mediated protection in the spleen against a subsequent heterologous infection by the Gram-negative pathogen *Salmonella* Typhimurium (*S*.Tm). Utilizing single cell RNA-sequencing and flow cytometry, we discerned STAT1-regulated genes in TI-associated resident and recruited splenic myeloid populations. The temporal dynamics of TI were further elucidated, revealing both early and delayed myeloid subsets with time-dependent, cell type-specific STAT1 signatures. Using lineage tracing, we find that tissue-resident red pulp macrophages (RPM), initially depleted by BCG exposure, are restored from both tissue-trained, self-renewing macrophages and from bone marrow-derived progenitors, fostering long lasting local defense. Early inhibition of STAT1 activation, using specific JAK-STAT inhibitors, reduces both RPM loss and recruitment of trained monocytes. Our study suggests a temporal window soon after BCG vaccination, in which STAT1-dependent activation of long-lived resident cells in the tissue mediates localized protection.

Introduction

Trained immunity (TI) is defined as the capacity of innate immune cells to recall and modulate their subsequent responsiveness following prior exposure to a diverse array of stimuli[1]. Unlike the adaptive immune system, these changes are antigen-agnostic and are more reflective of sustained alterations in cellular and systemic states. TI has been demonstrated to directly reprogram the metabolic, transcriptional, and epigenetic state of monocytes and macrophages, generating heightened inflammatory capabilities in-vitro[1,2]. As the transient lifespans of these cells are weeks only, this alone is insufficient to explain the sustained protection generated by TI that can last from months to years. To address this limitation, current research has been focused on long-lived multipotent progenitor immune cells.

BCG vaccine (Bacillus Calmette-Guérin), an attenuated strain of *Mycobacterium bovis*, is a potent inducer of TI, which facilitate nonspecific protection against heterologous pathogens in mice, primates, and humans[3,4]. The effects of intravenous (i.v.) BCG vaccination, where bacilli persist within the bone marrow (BM), drive the expansion of LSK+ hematopoietic stem cells (HSCs) and multipotent progenitors (MPPs)[4]. In conjunction, MPPs undergo biased differentiation towards myelopoiesis, increasing the proliferation of myeloid cells. These effects are driven primarily by interferon activation, particularly that of interferon-gamma (IFNγ) and its downstream transcription factors, STAT1 and IRF1, in MPPs and short-term HSCs, resulting in a transcriptional program of cell cycling (Cdk1, Cdk4, Ccnf) and histone modifications. Furthermore, these newly differentiated circulating cells have enhanced microbicidal properties[5,6]. Upon infection, in order to elicit protection against invading agents, trained progenitor immune cells from the BM interact within local immune cell compartments in the tissue. Understanding these mechanisms is particularly relevant given emerging challenges in infectious disease control. The rise of antimicrobial-resistant bacteria demand the development of attenuated strains-specific vaccines[5], such as the typhoid conjugate vaccine (TCV) for the gram negative *Salmonella* Typhi[6]. The premise of BCG and trained immunity is providing global heterologous protection against a range of pathogens. However, the broader potential of TI-mediated heterologous protection requires understanding of TI-mediated protection as it translates within the tissue and the local cellular architectures is not completely understood.

58 Most tissues harbor long-lived resident macrophages capable of self-renewal, independent of BM-
59 derived precursors. These resident populations, including pulmonary alveolar macrophages, Kupffer
60 cells in the liver and red pulp macrophages in the spleen, originate from embryonic erythro-myeloid
61 progenitors[7]. Antimicrobial activity of resident populations control early stages of invasion by pathogens
62 but are than depleted, and the niche is repopulated either by self-renewal[8] or by progenitors derived
63 from the BM to maintain local functions[9]. Intriguingly, resident alveolar macrophages (AM) have been
64 shown to undergo in-situ training, maintaining an altered phenotype over an extended period[10–12]. One
65 mechanism driving this training in-situ in AMs involves CX3CR1^{+} T cells, which have been implicated in
66 local reprogramming via IFNγ release. This process has been demonstrated to occur around three weeks
67 after initial BCG vaccination, after which interferon-driven responses occur across the organism,
68 including lung and BM, resulting in viral and mycobacterial protection. It remains unclear however, how
69 during TI, a bridge is formed between peripheral, resident cells and BM-derived recruitment of trained
70 myeloid cells.

71 In this study, we set out to investigate the interplay of circulating and tissue-level immune cells that
72 mediate protection and remodeling during TI. To induce tissue specific TI, we used a model of
73 intraperitoneal (i.p.) injection of BCG, which rapidly delivers the bacteria to target lymphatic organs
74 (*e.g.,* spleen), and measured protection against subsequent *Salmonella* Typhimurium (*S*.Tm) challenge.
75 Within the spleen's unique structure and cellular composition, we characterized STAT1-mediated, cell
76 type-specific TI signatures. We demonstrate that an initial depletion of resident red-pulp macrophages is
77 followed by repopulation by recruited trained monocytes and a local self-renewing population,
78 contributing to the maintenance of STAT1 signatures and long-lasting protection within the tissue.

79

80 Results

81 Intraperitoneal BCG results in heterologous *S*.Tm protection and a distinct myeloid subsets with 82 signatures driven by STAT1.

83 To establish an in-vivo BCG training model targeted to the splenic tissue, and assess the extent of cross
84 pathogen tissue protection conferred, we administered BCG-Pasteur[10] (5×10^{6} colony forming units
85 (CFU)) or PBS as a control via i.p injection to 8-week-old female C57BL/6J mice. Following a two-week
86 training period, mice were challenged with *S*.Tm ($5x10^{5}$ CFU) through i.p inoculation (**Fig. 1A**). Mice were

87 sacrificed after twenty-four hours, and spleen homogenates were cultured on LB agar medium to
88 quantify *S*.Tm load using CFU (**Fig. 1B**). Relative to the control group, mice that received BCG exhibited
89 enhanced protection against *S*.Tm, with a four- to five-fold decrease in CFU, indicating TI-mediated
90 splenic protection.

91 For identification of transcriptional changes in splenic myeloid populations related to TI, we isolated
92 splenocytes and performed staining with CD11b, Ly6C, and F4/80 gating for myeloid mononuclear
93 phagocytes (MPs), including classical monocytes (CM) ($CD11b^+Ly6C^+$), and $CD11b^+$ $Ly6C^-$ MPs comprising
94 non-classical monocytes (NCM) and conventional dendritic cells (cDC), and also resident red pulp
95 macrophages (RPM) ($CD11b^-$ $F4/80^+$) (**Fig. 1C**, **Figure 1 — figure supplement 1A**). We observed an
96 overall expansion of the myeloid compartment due to training, with an increase in the $CD11b^+$ subset,
97 and a pronounced reduction of resident RPM (**Fig. 1D**). This observed loss of RPM is common during
98 infection and inflammation and has been previously described as the resident macrophage
99 disappearance reaction[11].

100 We next determined transcriptional alterations caused by TI across the myeloid compartment. $CD11b^+$
101 cells from trained and naïve mice were isolated by sorting and processed for single-cell RNA-sequencing
102 (scRNA-seq)[12]. K-nearest neighbor (K-NN) clustering differentiated six distinct cell types, designated as
103 CM, NCM, immature DC2 (cDC2), mature DC2 (mcDC2), neutrophils, and NK cells (**Fig. 1E**). The identity
104 of each cell type cluster was based on established transcriptional markers (**Fig. 1F**). Additional analysis
105 was performed to identify differentially expressed genes (DEG) unique to training (**Fig. 1G-I; Table S1**).
106 While most populations derived from control or trained mice clustered together by cell type, we
107 identified a subset of trained CM (CM-T) particular to BCG (**Fig. 1G**). This subset represents an enhanced
108 state of the STAT1-regulated IFNγ response that characterizes trained CM (*e.g.*, *Gbp2, Ly6a, Cxcl9*, and
109 *Irg1)* (**Fig. 1J**). Notably, these STAT1 activated genes are known to drive maturation and activation of
110 monocytes and macrophages, enhancing their antimicrobial response[13].

111 *Stat1* and its downstream targets (*e.g.*, *Gbp2*, *Irf1,* and *Ly6a*), exhibited a pronounced elevation also in
112 other myeloid cells (**Figure 1 — figure supplement 1B**), aligning with an earlier report that BCG induces
113 BM and HSC remodeling via interferon signaling, resulting in STAT1 upregulation in progenitors[14].
114 However, not all populations were similarly activated in conjunction with STAT1-regulated genes, with
115 gene set enrichment analysis (GSEA) demonstrating differential pathway upregulation across cell types
116 (**Fig. 1I**). CM and mcDC2 primarily activated the IFNγ response, while complement associated genes

117 were enriched in mcDC2. NK cells alone showed minimal activation due to training across all detected
118 pathways (**Figure 1 — figure supplement 1B**).

119 We also observed increased SCA-1 (*Ly6a/e*) expression across the monocyte subsets and mcDC2, most
120 notably in NCM (**Fig. 1F**; **Figure 1— figure supplement 1B**). SCA-1 (stem cell antigen-1) is a
121 glycosylphosphatidylinositol-anchored cell surface protein commonly used as a marker for murine
122 hematopoietic stem and progenitor cells within the BM. The STAT1 signaling pathway has been shown
123 to be involved in the regulation of SCA-1 expression[15], suggesting a role for STAT1 in the modulation of
124 SCA-1 during development of TI. Recent studies have also demonstrated a link between SCA-1 and
125 inflammation, with its expression found to be upregulated on a specific subset of $Ly6C^+$ monocytes
126 during infection[16]. These $SCA\text{-}1^+$ monocytes exhibited a pro-inflammatory phenotype, characterized by
127 the production of inflammatory cytokines and chemokines, and were implicated in the amplification of
128 these responses. For $Ly6C^-$ NCM, the role of SCA-1 has not yet been studied.

129 In addition to the upregulation of inflammatory and antimicrobial genes, we also observed a significant
130 downregulation of specific genes in CM-T as a result of training, including *Ccr2*, *S100A8/9,* and *Ngp* (**Fig.**
131 **1J**). CCR2, a chemokine receptor crucial for monocyte recruitment, was found to be downregulated in
132 response to IFNγ. This reduction in CCR2 expression is mediated by IFNγ-induced mRNA instability,
133 potentially serving to retain monocytes at the site of recruitment and dampen a positive feedback
134 loop[17]. Similarly, BCG has been shown in other contexts to reduce the expression of S100A8 and S100A9,
135 two calcium-binding proteins that can heterodimerize and stimulate IFNγ production in CD4+ T-cells via
136 an IL-10 dependent mechanism[18]. By suppressing their activity, runaway signaling and exhaustion is
137 avoided. Lastly, NGP (neutrophilic granule protein), has been implicated in the regulation of
138 inflammation through its ability to block NF-κB signaling[19]. The downregulation of these genes suggests
139 that trained immunity not only enhances pro-inflammatory responses but also modulates the
140 expression of key regulators to maintain a balanced immune response and prevent excessive
141 inflammation.

142

143 **Dynamics of TI-associated subsets and signatures indicates early and delayed kinetics**.

144 To gain insight into dynamic processes underlying splenic cell type-specific TI, we conducted a two-
145 month experiment, sacrificing mice at days 3, 14, 30, 45, and 60 post-vaccination with BCG, and
146 challenging with S.Tm at 14 and 60 days post training (**Fig. 2A**). We assessed BCG growth in BM and

147 spleen, resistance to *S*.Tm infection, flow cytometry analysis with cell type-specific training markers
148 (CXCL9 and SCA-1), and bulk RNA-seq. Notably, protection against *S*.Tm persisted for two months post-
149 vaccination, albeit with waning resistance over time (**Fig. 2B**). While intravenous (i.v) BCG delivery and
150 subsequent localization of the bacterium to the BM were previously noted as crucial for robust
151 training[14,20], our results indicate that during i.p administration this process is dispensable, as no BCG
152 were detected in the BM (**Fig. 2C**). Conversely, in the spleen, we isolated BCG at all time points, with CFU
153 declining sharply by day 14, reaching the limit of detection by day 30 with minimal bacterium remaining
154 (**Fig. 2C**).

155 Flow cytometry analysis revealed a dynamic process during trained immunity (**Figure 2— figure**
156 **supplement 1A**). Compared to mean control values, we observed rapid recruitment of CMs in the
157 spleen, starting already at day three after BCG, peaking at day 14 before returning to baseline (**Fig. 2D**,
158 **Figure 2—figure supplement 2B**). We also stained cells for CXCL9 expression, as a marker gene of
159 STAT1-mediated TI that defines the CM-T subset, and revealed that this population reaches peak levels
160 at day 14 (**Figure 2— figure supplement 1C**). In a separate experiment to assess early kinetics of CM-Ts,
161 we measured a significant increase of this subset already at five days post BCG (**Figure 2— figure**
162 **supplement 1D**), indicating an early recruitment of these cells due to the initial response to BCG. NCMs
163 exhibit a different TI signature and kinetic pattern. While their ratio initially declines, they return to
164 steady-state levels by day 30 (**Fig. 2D**). NCMs express SCA-1 (*Ly6a*), another STAT1-regulated gene,
165 which persists and remains highly elevated at all subsequent time points (**Figure 2— figure supplement**
166 **1C**). Challenge with S.Tm at day 14 triggered an expansion of CM-Ts, but this response was lost by day
167 60, coinciding with the diminished protection observed at this later timepoint (**Figure 2— figure**
168 **supplement 1E**). In contrast, SCA-1 expression in NCMs remained upregulated (**Figure 2— figure**
169 **supplement 1E**).

170 Notably, the expression of STAT1-mediated TI markers is not solely restricted to BM-derived myeloid
171 cells but also occurs in tissue-resident RPM. RPM loss is evident after 14 days of training (**Fig. 2D**),
172 together with increased expression of the STAT1-regulated CXCL9 (**Figure 2— figure supplement 1C, D**).
173 SCA-1^{+} RPM levels fluctuate, elevating at day 14 and increasing again at day 60. Given their pivotal role
174 in curbing the early replication of intracellular pathogens[21], such as *S*.Tm, and their long life span, as
175 opposed to CM and NCM[22], trained RPM could be an additional determinant in generating long-lasting,
176 localized tissue protection.

177 From the splenocytes collected during the kinetics experiment, we generated and analyzed bulk RNA-
178 seq data. Principal component analysis (PCA) displayed a substantial shift along PC1 due to BCG training
179 (**Figure 2— figure supplement 1F**). Examination of all differentially expressed genes (DEGs) between
180 BCG and PBS across these time points revealed the greatest transcriptional changes at day 14 and 30
181 (**Fig. 2E; Table S2**).

182 To investigate the biological processes represented at these time points, GSEA was performed. At day
183 14, we detected enrichment for IFNγ response, IFNα response, and IL6-JAK-STAT signaling, with many
184 genes shared across these pathways (**Fig. 2F**). This STAT1-dependent program includes several
185 interferon-regulated genes upregulated at day 14, including the *Gbp* gene family, *Ifitm3*, and *Socs3* (**Fig.**
186 **2G**). GBPs are guanylate-binding proteins involved in antimicrobial activity and inflammasome
187 activation[23], while IFITM3 is an interferon-induced transmembrane protein that plays a role in the
188 antiviral response[24]. SOCS3, a suppressor of cytokine signaling, particularly via IL-6/STAT3, is a necessary
189 component for mycobacterial infection control. By blocking IL-6 signaling, SOCS3 allows for TNF and IL-
190 12 signaling to occur, initiating CD4-dependent IFNγ release[25].

191 Within the IFNγ response pathway, we noted that associated genes display distinct temporal expression
192 patterns. For example, *Irg1* upregulation is limited to day 14 (**Figure 2— figure supplement 1G**)
193 returning to control values for all subsequent time points. This may reflect that IRG1 induction requires
194 bacterial phagocytosis and activation of the TLR-2/MYD88/NFKB axis[26]. Conversely, an increase in *Cxcl9*
195 expression is already observed by day 3, plateauing at day 14, and decreasing by day 30, mirroring its
196 induction in CM-Ts in the flow cytometry analysis. Curiously, despite its loss in CM-Ts, the bulk
197 transcriptional expression of *Cxcl9* is still sustained after 2 weeks, though at reduced levels. This may be
198 attributed to its activity in other immune cells or regulatory mechanisms preventing further translation.
199 Importantly, the IFNγ response mirrored STAT1 activity, showing initial reduction after 2 weeks followed
200 by sustained upregulation for all subsequent time points (**Fig. 2H**), reinforcing their coupled role in
201 mediating the effects of TI. Other downstream targets of STAT1, including *Ly6a* (SCA-1), maintain high
202 expression 2 months post vaccination (**Figure 2— figure supplement 1G**).

203 Distinct from these immune signatures, day 30 was characterized by enrichment of E2F targets, G2M
204 checkpoint, and heme metabolism (**Fig. 2E, F**). Interestingly, RPM play a crucial role in iron homeostasis,
205 recycling and storing iron from senescent erythrocytes, preventing accumulation of free iron that can
206 lead to ROS production, oxidative damage, and pathogen utilization[27]. Given the dynamics of RPM loss
207 by day 14, it is tempting to speculate that their subsequent repopulation is reflected by these processes.

208 We then investigated whether TI signatures could be maintained through progenitor programming
209 alone. BCG or PBS were injected i.p into mice with either a CD45.1 or CD45.2 background, respectively
210 (**Figure 2— figure supplement 1H**). After two weeks, BM was harvested from both, HSCs mixed 1:1, and
211 injected into irradiated mice for BM transplant. Six weeks post transfer, mice were sacrificed and
212 myeloid cells in the spleen were assessed (**Figure 2— figure supplement 1I**). Within each mouse, we
213 found in the spleen a greater fraction of NCMs expressed SCA-1 from trained donors relative to the
214 naïve control (**Figure 2— figure supplement 1J**). This persistence of the training signature in a naive host
215 environment demonstrates that SCA-1 expression in NCMs can be maintained through progenitor
216 programming alone, though it does not exclude potential contributions of local tissue signals during
217 normal BCG training. CM-Ts however, were undetectable, consistent with the transient nature of this
218 subset observed in our kinetics data.

219 **RPM niche is replenished by recruited trained monocytes and by local training of tissue-resident**
220 **populations**.

221 We observed a substantial reduction in RPM numbers upon BCG, followed by the expression of STAT1-
222 mediated TI markers in RPMs. We hypothesized that upon BCG, two possible scenarios for training and
223 replenishment of open niche are possible. The first is self-renewal by the remaining local tissue-resident
224 macrophages who are trained within the tissue, while the other is that BM-derived trained monocytes
225 differentiate and repopulate the open niche. While BM-derived macrophages may adopt signatures and
226 function of their local counterparts, they may also retain aspects of their origin, particularly enhanced
227 inflammatory capacities (**Fig. 3A**). To investigate this, we employed MS4A3^{Tdtm};CX3CR1^{GFP} reporter
228 mice[28] with a knock-in flox-cre system to selectively label BM-derived monocytes with TdTomato
229 fluorescence. As MS4A3 is distinctly expressed in granulocyte-monocyte progenitors (GMP), only this
230 lineage will be TdTomato positive. These mice were administered BCG or PBS-i.p following the training
231 protocol and sacrificed two weeks later (**Fig. 3B**). Effective labeling was determined by flow cytometry,
232 measuring the fraction of MP expressing TdTomato and/or CX3CR1 (**Figure 3— figure supplement 1A**).
233 As expected, the monocyte population were primarily double positive (**Figure 3— figure supplement**
234 **1B**). Intriguingly, training increased the percentage of labeled cells across monocytes, suggesting a
235 potential lineage bias towards granulocyte-monocyte progenitors (GMPs). This observation is consistent
236 with prior studies demonstrating that various microbial components can induce short-term
237 differentiation biases in monocytes derived from GMPs or MDPs (monocyte-dendritic progenitors),
238 endowing them with neutrophil- or dendritic cell-like properties[29].

239 For the majority of RPM, we expected minimal TdTomato expression, representative of self-
240 replenishment during homeostasis. However, already within the control we observed that ~16% of the
241 population were labeled (**Fig. 3C**). When this population was depleted during training, an even greater
242 fraction was positively labeled. Accordingly, even under steady-state conditions, BM-derived cells
243 contribute to the resident niche, but when sufficiently diminished post vaccination, active
244 replenishment from the BM does occur.

245 To determine whether Tdtm$^+$ BM-derived RPM acquired a distinct transcriptional profile due to training
246 compared to the native Tdtm$^-$ population, we sorted Tdtm$^+$ RPMs, Tdtm$^-$ RPMs, and Tdtm$^+$ CM and NCM,
247 from both trained and naïve conditions. These sorted cell populations were then subjected to bulk RNA-
248 seq and subsequent analysis. Crucially, training associated genes were differentially expressed across all
249 sorted cell types (**Fig. 3D**; **Figure 3— figure supplement 1C; Table S3**). When evaluating specific DEGs
250 upregulated across trained RPM, we identified five gene clusters that varied between CM, NCM, and
251 RPM, as well as genes primarily upregulated in Tdtm$^+$ or Tdtm$^-$ RPM (**Fig. 3E**). Cluster I is composed of
252 MHCII-associated genes (*H2-Aa*, *H2-Eb1*, CD72, etc.), and is enriched in NCM and RPM cells, indicating
253 enhanced antigen presentation that may facilitate the activation of humoral immunity. Cluster II consists
254 of the STAT-1 regulated TI hallmark genes, including *Cxcl9*, *Gbp2* and *Stat1* and is upregulated in all
255 trained subsets. Genes in Cluster III, such as *Aif1*, *Fpr1*, and *Hk3*, are primarily observed in trained RPM
256 and are involved in response to tissue damage/disruption and immune infiltration. AIF1 is an established
257 marker of macrophage activation and is functionally involved in phagocytosis and membrane ruffling[30].
258 Similarly, FPR1, a formyl peptide receptor, induces chemotaxis, phagocytic uptake, and reactive oxygen
259 species (ROS) production[31]. Cluster IV is upregulated in BCG Tdtm$^-$ RPM, though the role of most genes
260 detected in this cluster remains unknown in regard to their tissue-specific function and activation.
261 Interestingly, *CD8A* expression, typically relegated to lymphocytes, was observed in this cluster. In
262 monocytes, CD8A can co-engage with FcR, resulting in TNF release[32]. Lastly, cluster V, which is primarily
263 activated in CM regardless of training, was also upregulated in RPM due to BCG. Three of the genes
264 within the cluster, *Anxa1*, *Vim*, and *Wfdc17*, have all been shown to dampen excess inflammatory
265 responses through various mechanisms, including suppressing oxidative stress and promoting local
266 resolution[33–35].

267 GSEA performed across all upregulated genes revealed that the IFNγ response was enriched, followed by
268 IFNα response, allograft rejection, and JAK-STAT signaling (**Fig. 3F**). Although the IFNγ signature was
269 most prominent in CM, it was also observed in NCM and in the Tdtm$^+$ RPM. This finding suggests that

270 engrafted monocytes differentiating within the niche may maintain a more inflammatory phenotype
271 and a heightened sensitivity to IFNγ activation. However, the BM-derived RPM are not the sole
272 population responsive to training, as the local fraction also upregulates the same genes in clusters I-III.
273 Notably, RPM, as a whole, demonstrate a greater capacity to upregulate the expression of many
274 interferon genes, including *Cxcl9* and *Stat1* (**Figure 3— figure supplement 1D**). Taken together, our
275 results indicate that BCG can reprogram populations and generate training via two separate routes.
276 First, the recruitment of trained progenitors and monocytes within the spleen, which differentiate
277 within a vacant niche, retaining their trained identity. Second, activation directly within the spleen in the
278 context of native tissue-resident RPM, generating tissue-specific protection.

279

280 **Transient IFNγ-STAT1 inhibition prevents TI signatures and splenic infection resistance.**

281 We observed that STAT1 signaling holds a critical role in training, with its regulated gene expression
282 elevated across the myeloid population. However, BCG is an intact attenuated bacterium that can
283 activate numerous PRRs. To evaluate whether STAT1 is necessary for TI signatures and protection, we
284 vaccinated STAT1-KO mice[36] with either PBS or BCG-i.p (**Figure 4— figure supplement 1A**). After a two-
285 week period, we assessed the myeloid population and STAT1 regulated genes. We observed a complete
286 absence of expression for both CXCL9 and SCA-1 across myeloid populations (**Figure 4— figure**
287 **supplement 1B**). This aligns with previous findings that demonstrated compromised acquisition of
288 trained immunity in IFNγR$^{-/-}$ mice[14]. Interestingly, RPM, typically depleted following BCG inoculation,
289 remain preserved in STAT1-KO mice (**Figure 4— figure supplement 1C**), suggesting that STAT1-mediated
290 pathways are involved in triggering the cellular death processes that occur during BCG interaction
291 and/or engulfment.

292 There is however a significant limitation in this mouse model, as STAT1$^{-/-}$ leave mice highly susceptible to
293 infection due to a severe compromise of immune homeostasis, limiting our ability to assess TI-mediated
294 protection upon *S*.Tm challenge. In light of our findings that STAT1 signaling is activated shortly after
295 BCG administration, we sought to transiently restrict STAT1 activity at these early time points, also
296 enabling us to investigate the effect of inhibition of STAT1 signaling on training and protection, without
297 affecting STAT1 activation during a secondary *S*.Tm challenge. To accomplish this, we used Fedratinib, a
298 specific inhibitor of JAK2 activation of STAT1 through IFNγ signaling[34], and Deucravacitinib, a specific
299 inhibitor of TYK2 activation of STAT1/STAT2 through IFNα/β signaling[37]. First, we administered DMSO

300 (control), Deucravacitinib, and Fedratinib i.p followed by BCG or PBS-i.p four hours after. These
301 inhibitors were then injected daily via i.p for the following four days, followed by a subsequent nine-day
302 rest period (**Figure 4— figure supplement 1D**). At the two-week mark, splenocytes were extracted from
303 all mice and analyzed by bulk RNA-seq. Only Fedratinib, not Deucravacitinib, resulted in inhibition of
304 STAT1-mediated TI signatures (**Figure 4— figure supplement 1E; Table S4**).

305 We then repeated this experiment, focusing on training phenotypes in the spleen and BM. At the two-
306 week mark, splenocytes were extracted from all mice for flow cytometry analysis, with CXCL9 utilized as
307 a marker for STAT1-mediated TI signature in CM-Ts. As observed in the transcriptional response, only
308 Fedratinib ablated the CXCL9^{+} CM-Ts (**Figure 4— figure supplement 1F**). We also sought to determine if
309 these effects were localized solely to the tissue, or if they extended to progenitors in the BM, which
310 expand upon BCG exposure[14]. To ascertain this, we isolated BM from the femur, measuring the percent
311 of LSK^{+} HSCs (**Figure 4— figure supplement 1G**). Here too, only Fedratinib resulted in suppressing their
312 expansion to levels comparable to the control (**Figure 4— figure supplement 1H**). Conversely,
313 perturbation of IFNα/β signaling with Deucravacitinib lead to no observable changes on trained subsets,
314 suggesting that it is not involved in our BCG-i.p model. Type-I interferon has been established as a
315 training signaling pathway in other contexts, as observed with β-glucan[38], *Candida Albicans*[39] and LPS[40].

316 In order to prove that early STAT1 inhibition is sufficient to block the TI protective phenotype, and not
317 just downstream markers, we repeated the inhibitor regime with control or trained mice receiving
318 either Fedratinib or DMSO, with or without *S.*Tm infection after 2 weeks (**Fig. 4A**). We then extracted
319 spleens to measure splenic expansion, splenoctye population levels and marker expression with flow
320 cytometry, bulk splenocyte transcription, and *S.*Tm susceptibility. Importantly, while we observed no
321 differences in CFU between control mice with or without Fedratinib, trained mice receiving Fedratinib
322 were significantly more susceptible to infection (**Fig. 4B**). Treatment with Fedratinib resulted in
323 diminished recruitment and splenocyte expansion, causing an appreciable reduction in spleen size
324 comparable to the control (**Figure 4— figure supplement 1I**). Accordingly, the balance of monocytes
325 ratios, particularly NCM, was shifted to levels similar to those observed in the DMSO control (**Fig. 4C**). In
326 conjunction, the frequency of CXCL9^{+} CM-Ts was diminished, reflecting a reduction in the subset, while
327 in RPMs, CXCL9 showed decreased expression (**Fig. 4D**). Finally, RPM, which typically undergo depletion
328 after training, exhibited significantly enhanced survival, similar to the observations in STAT1-KO mice
329 (**Fig. 4C**).

330 To probe the effects of Fedratinib inhibition beyond myeloid expansion and marker acquisition, we
331 conducted bulk RNA sequencing on total splenocytes isolated from all experimental conditions. PCA of
332 the resulting data revealed two major axes of divergence among the populations: PC1, associated with
333 training, and PC2, associated with the response to *S*.Tm (**Figure 4— figure supplement 1J**). While the
334 PBS-i.p mice treated with either DMSO or Fedratinib were grouped together, the BCG-i.p samples
335 treated with Fedratinib clustered distinctly, shifting closer to the PBS control group. Analysis of
336 downregulated DEGs identified the IFNγ response as the most significantly affected pathway due to
337 JAK2 inhibition by Fedratinib. This included its downstream effector *Stat1*, and other key STAT1-
338 regulated trained immunity genes, such as *Cxcl9/10*, *Irf1*, *Gbp2*, and *Irg1*, across all treated mice (**Fig. 4E,**
339 **F; Table S5**). To further validate our findings and ensure that the loss of the trained immunity signature
340 was not solely a result of blocking other JAK2-associated pathways, we repeated the inhibitor
341 experiment using recombinant α-IFNγ. Mice were given either α-IFNγ or an isotype control after BCG or
342 PBS vaccination, with injections on days 0, 2, and 4, and assayed two weeks post-vaccination. Upon
343 sorting and sequencing CM and RPM from these treated mice, we found that the STAT1 regulated TI
344 signatures were completely ablated with early inhibition (**Figure 4— figure supplement 1K-L**). Although
345 we measured no changes in viable BCG in cultured spleen homogenates from control and treated mice
346 at the two-week interval (**Figure 4— figure supplement 1M**), early α-IFNγ was sufficient in blocking
347 training signatures. Interestingly, previous studies show that while removal of BCG by long term
348 antibiotic treatment decreases expansion of progenitor cells, protection against secondary ex-vivo
349 challenges remains[14].

350 Thus, the impact of Fedratinib and α-IFNγ treatment on the TI phenotype further underscores the
351 pivotal role of IFNγ and the JAK2-STAT1 axis in orchestrating the early programs and signatures required
352 for long-term local and recruited myeloid populations within the tissue. When compromised,
353 remodeling is suppressed and so too protection. Crucially, even though its administration was early and
354 removed after only five days administration, inhibition occurred. This indicates that the acquisition of TI
355 in the tissue occurs within a critically narrow temporal window.

356

357 Discussion

358 TI, or innate immune memory, embodies the capacity of innate immune cells to remember past
359 encounters and modify their subsequent responses, triggered by diverse conditions and stimuli. In-vivo

360 these processes are sustained in progenitor cells within the BM to provide long term TI, with
361 differentiated cells inheriting this memory[14,41]. In this study, we set out to demonstrate how long-term
362 protection events in the BM affords training within the tissue through local interactions with resident
363 populations. We demonstrated how the immune effects of BCG vaccination are differentially imparted
364 across recruited trained monocytes from the BM and diverse MP populations within the spleen, the
365 temporal dynamics governing these processes, and the mechanisms necessary for them to be sustained
366 long-term.

367 We verified that BCG-i.p inoculation stimulates an expansion of myeloid MP, notably a subset of classical
368 monocytes marked by CXCL9 expression (CM-T) within the spleen. This CM-T population, which peaks at
369 day 14 before declining, exemplifies the broader training response we observed, as our dissection of
370 single-cell training signatures uncovered a fundamental program dominated by IFNγ response and
371 STAT1 regulated genes across diverse populations. Among these, GBP2, CXCL9, and IRG1 represent
372 some of the pathways involved in the protective response: GBP2, a member of the GTPase family, drives
373 macrophages toward an inflammatory state[42] while combating bacterial infection through vacuole
374 disruption and pyroptosis induction[43]. CXCL9 orchestrates immune cell recruitment and activation at
375 infection sites[44], supporting trained immunity by establishing a pro-inflammatory environment
376 conducive to pathogen clearance[45]. Meanwhile, IRG1 produces the metabolite itaconate, which serves
377 dual functions in both directly inhibiting pathogen growth and modulating immune responses to prevent
378 excessive inflammation[46,47]. However, IRG1's role in training appears context-specific, as exposure to
379 training stimuli like β-glucan can actually block its activity[48].

380 By monitoring the kinetics of training over an extended duration, we observed that the initial surge in
381 CM recruitment is confined to the first two weeks of training, potentially signaling inflammatory
382 recruitment triggered by BCG exposure and RPM loss. Concurrently, the presence of CM-Ts starts to
383 diminish at a similar rate and is eventually lost, suggesting that these cells may be differentiated to
384 trained MPs in the tissue.

385 The depletion of RPMs at 14 days post-vaccination sets in motion a series of complex cellular responses.
386 Notably, we observed an enrichment of heme metabolism at day 30, which may indicate an ongoing
387 process of RPM replenishment. This process typically involves two key mechanisms: the local expansion
388 and repopulation by native populations, and the recruitment of erythroid and myeloid progenitors,
389 including classical and non-classical monocytes, to the organ[49]. These recruited cells, particularly
390 monocytes, can differentiate within the niche, transitioning through a pre-RPM state via heme-mediated

391 pathways[50]. Interestingly, heme metabolism has also been implicated in the control and pathogenicity of
392 mycobacterial species, particularly *Mycobacterium tuberculosis* (MtB). During systemic infection, MtB
393 activates type I interferon (IFN-I) signaling, which, along with its own virulence factors, disrupts iron
394 transport and uptake[20].

395 The presence of TI markers not only in BM-derived myeloid cells such as CM and NCM, but also in RPM,
396 prompted us to uncover how these cells acquired this phenotype. Utilizing Ms4a3^{TdTm} labeled mice, we
397 investigated whether trained RPM were being derived from cells originating in the BM. Unlike CM and
398 NCM, which are predominantly TdTm^{+}, RPM express this lineage tracing marker at steady state around
399 16%, which was further increased with training. Probing the transcriptional profile of these cells also
400 revealed differences due to origin, with Tdtm^{+} RPM demonstrating a heightened response to IFNγ
401 stimulation and elevated expression of STAT1. However, both populations exhibit significant
402 upregulation of TI-associated genes post-vaccination. These findings indicate that TI in RPM is not solely
403 due to BM-derived precursors filling a depleted niche but suggests a capacity for both resident and BM-
404 derived RPM to undergo training within the tissue itself. Considering the importance of these cells in
405 restricting early infection events[21], their capacity for training reveals an additional factor contributing to
406 the TI phenotype. While our examination was limited to a singular tissue-resident macrophage subset,
407 other splenic macrophages like marginal zone macrophages (MZMs) and marginal metallophilic
408 macrophages (MMMs), known to have immunological roles, may similarly exhibit a capacity for being
409 trained. This research can be further broadened to include other resident myeloid populations, to
410 explore how BCG can bestow localized protection independent of central HSC reprogramming.

411 When investigating the longevity of the trained transcriptional response within the spleen, we noted
412 that *Stat-1* and other interferon response genes remained upregulated even two months after
413 vaccination. We found one such gene SCA-1 (*Ly6A*), was continuously expressed in NCM due to training,
414 and was still identifiable after a BM transplant. Although SCA-1 is traditionally a marker for upstream
415 progenitors, recent studies link its expression to inflammation, with upregulation noted in B/T cells
416 during *Mycobacterium Tuberculosis* (Mtb) infection[51]. Further exploration is warranted to investigate the
417 mechanisms that enable such enduring expression, particularly in this cell type. Also, while *Ly6a* (SCA-1)
418 is unique to mice, a recent study identified a human equivalent termed *Ly6s*, primarily expressed in
419 splenic NCM and regulated by interferon signaling, that was linked to an inflammatory cell phenotype
420 with resistance to viral infections[52].

421 Prior publications have demonstrated the importance of BCG localization in generating local vs. systemic
422 changes[14,53], and that BCG's initial presence within the BM is associated with HSC reprogramming and
423 long-term TI. Despite this, while we were able to isolate BCG from splenic tissue, not BM, from all
424 sampled time points, we could still achieve training and protection, including LSK^+ subset expansion in
425 the BM. This leads us to hypothesize that the signaling initiated due to BCG can act in trans, affecting
426 system wide changes, and is not solely acquired due to local pathogen interactions in the BM.
427 Supporting this, recent findings suggest that training in alveolar macrophages can also occur through
428 subcutaneous BCG administration, potentially acting via the gut-lung axis[54].

429 Finally, given STAT1's ubiquity among all trained cells, we hypothesized that this transcription factor and
430 its upstream activation via interferon signaling were instrumental in driving BCG-induced trained
431 immunity. We observed that early transient inhibition, specifically targeting IFNγ-mediated STAT1
432 activation, effectively negated the hallmarks of trained immunity. These include myeloid recruitment,
433 disappearance of RPM, the expression of training markers, LSK^+ expansion, transcriptional alterations,
434 and, crucially, heterologous *S*. Tm protection - highlighting STAT1's particular role in orchestrating a
435 protective response against this pathogen. Furthermore, while it is generally known that BCG can reside
436 within the tissue for weeks after inoculation, our findings suggest that even brief STAT1 and IFNγ
437 inhibition is sufficient to disrupt the development of trained immunity, regardless of the pathogen's
438 presence. It is plausible that during the initial stages of BCG exposure and inflammation, IFNγ-secreting
439 cells such as T/NKTs initiate the immunological remodeling needed for training. Should these processes
440 be obstructed at this critical juncture, the opportunity for subsequent training is lost. While our inhibitor
441 protocol was applied for a period of five days, the minimal duration required for effective inhibition and
442 comparable outcomes may be even shorter.

443 In summary, our study emphasizes that examining the tissue, specifically the spleen, as a tissue for
444 probing TI offers valuable insights into the temporal dynamics and signaling cascades that instigate and
445 sustain TI locally, in parallel with established systemic effects. Central to these processes is the IFNγ-
446 STAT1 pathway, which we identified as a key driver in establishing TI, by replenishment of resident naïve
447 MPs with trained recruited and local immune populations. We further delineated that during
448 intraperitoneal vaccination the resultant immune interactions limit BCG dissemination, while still
449 effectively eliciting training. Our findings open new avenues to harness STAT1 pathway induction for
450 optimized training and the importance of vaccines that can induce robust cross-domain protection.

451

454 # Methods

455 ## Experimental Methods

456 ### Mice and bacteria strains

457 C57BL/6J mice, 7-9 weeks old, were purchased from ENVIGO, housed at the Weizmann Institute
458 pathogen-free facility, and provided with standard food and water ad libitum. The Nr4a1 super-
459 enhancer sub-domain E2-KO ($E2^{-/-}$ or ^{C57BL}/6-*Rr39*^{em1Ched}/J) mice were purchased from The Jackson
460 Laboratory (#030204)[55]. The mice strains below were kindly provided by the following investigators:

461 - STAT1-KO mice by Prof. Dr. Mathias Müller[36].
462 - Ms4a3Cre^{TdTomato}-CX3CR1^{GFP} and CD45.1 mice by Prof. Steffen Jung.

463 All experiments were performed in accordance with the guidelines outlined by the Weizmann Institute
464 Committee on Animal Care.

465 For in-vivo training, BCG-Pasteur, generously donated by Dr. Daniel Barkan, was utilized. The *Salmonella*
466 *enterica* serovar Typhimurium strain SL1344 was used exclusively for all infection challenge experiments.

467 ### Mice training and infection

468 BCG were grown in Middlebrook 7H9 media (BD) supplemented with Middlebrook OADC (BD) at 37°C
469 for 1 week to stationary phase. Bacterial aliquots of 1mL were dispensed to 2mL cryotubes (Simport)
470 and frozen at -80C for long term storage. Prior to inoculation, tubes were thawed, centrifuged (10,000g,
471 2 min, RT), with pellet resuspended in 1 mL phosphate-buffered saline (PBS) (Sartorius). Bacterial
472 concentration was calculated based on optical density at 600nm (OD_{600}) assuming a concentration of
473 $5x10^8$ CFU/OD, with BCG diluted to $25x10^6$ CFU/mL in PBS. Mice were injected intraperitoneally (i.p)
474 with 200μl containing $5x10^6$ CFU or PBS (as controls). At given time points, mice were euthanized by CO_2,
475 spleens and/or BM from the femur were harvested, and CFU numbers were evaluated by plating serial
476 10-100-fold dilutions of homogenized spleens or BM suspension on selective 7H9-Middlebrook agar
477 plates.

478 For the initial challenge as observed in Fig.1A, cultures of S.*Tm* were grown in Luria-Bertani (LB) medium
479 (BD) at 37°C for 16 hours to stationary phase. For all subsequent experiments, S.*Tm* were grown at 37°C
480 for 16 hours to stationary phase in SPI-2 inducing media[56]: MgMES media (170 mM 2-(N-morpholino)
481 ethanesulfonic acid (MES) at pH 5.0, 5 mM KCl, 7.5 mM (NH4)2SO4, 0.5 mM K2SO4, 1 mM KH2PO4, 8

482 mM MgCl2, 38 mM glycerol, and 0.1% casamino acids. Cultures were centrifuged (10,000g, 2 min, RT),
483 with pellet resuspended in PBS. Bacteria were diluted 10-fold in PBS and concentration calculated based
484 on optical density at 600nm (OD_{600}). Assuming a concentration of $1x10^9$ CFU/OD, S.*Tm* was diluted to
485 $2.5x10^6$ CFU/mL in PBS. Mice were injected intraperitoneally (i.p) with 200 µl containing $1x10^5$ CFU of
486 bacteria or PBS (as controls). Injected bacterial load was verified by CFU. 24 hours post infection, mice
487 were euthanized by CO_2, spleens were harvested, and CFU numbers were evaluated by plating serial 10-
488 100-fold dilutions of homogenized spleens on streptomycin LB agar plates.

489 **BCG CFU**

490 Spleens or BM were homogenized and serially diluted in PBS + 0.1% Triton on 7H9 Middlebrook media +
491 OADC with Zeocin and Kanamycin. Plates were incubated for three weeks in a humidified 5% CO^2
492 incubator, with CFU determined using an automated colony counter.

493 **In-vivo interferon inhibition**

494 JAK-STAT inhibitors Fedratinib (cat #202893), and Deucravacitinib (cat #555349) (MedKoo Biosciences)
495 were resuspended in DMSO, aliquoted, and stored at -80C for later use. For injection, a mixture of PEG-
496 300 (Sigma):Tween-80 (Sigma) was prepared at a ratio of 18:1 and filtered using a 0.22 µm filter. For
497 each injection, 10µl of DMSO with or without the inhibitor was added to 105 µl of the PEG:Tween mix,
498 followed by 180µl of PBS for a total of 30µl and injected i.p. Inhibitor concentrations are 1mg and 0.5mg
499 per mouse for Fedratinib and Deucravacitinib respectively. Four hours post inhibitor, BCG or PBS-i.p was
500 injected for training. Daily repeat injections of the inhibitors were repeated for four additional days.

501 For the antibody inhibition experiment, 1mg of monoclonal αIFNγ antibody (clone: XMG1.2) or isotype
502 control (clone: Rat IgG1) was injected i.p. four hours pre BCG vaccination (day 0), then every other day
503 (day 2 and 4).

504 **Splenocytes and BM isolation and flow cytometry preparation**

505 Spleens and BM from femurs were extracted and stored in cooled FACS Buffer (PBS, 10 mM EDTA, 2%
506 FBS) until further extraction.

507 For BM extraction, femurs were cut at both ends and placed in 0.5mL microfuge tube with a small hole
508 in the bottom cut out using an 18G needle. This tube was then placed in a 1.5mL microfuge tube and
509 centrifuged (3 min, 500g, 4°C). The pellet was resuspended in red blood cell (RBC) lysis buffer for 4
510 minutes at room temperature, centrifuged (3 min, 500g, 4°C) and re-suspended with FACS buffer. For

511 CFU determination, suspension is used directly for serial dilution. For further flow cytometry processing,
512 FACS buffer containing CD16/CD32 blocking antibodies (BioLegend) is added for a 15-minute incubation
513 on ice. All subsequent processing is identical to splenocytes.

514 The spleens were dissected, mashed against a 70μm cell strainer (Falcon) and washed with 5mL of cold
515 FACS buffer. 1mL of splenocytes were aliquoted to microfuge tubes and centrifuged twice (3 min, 500g,
516 4C). Pellets were re-suspended with RBC lysis buffer (Sigma), incubated for 4 minutes at room
517 temperature, centrifuged (3 min, 500g, 4C) and re-suspended with FACS buffer containing CD16/CD32
518 blocking antibodies (BioLegend) for 15 minutes on ice. Cells were centrifuged once more, and pellets
519 were transferred to wells of a 96-well low attachment plate for multi-sample preparation. Subsequently,
520 fluorophore-conjugated antibodies cocktails (listed below) in Brilliant Stain Buffer (BD) were used to
521 resuspend pellets, followed by a 30-minute incubation on ice. Cells were washed, re-suspended with
522 500-1000μl FACS buffer and passed through a 35μm cell strainer (Falcon). For absolute quantification of
523 cell populations, 10-50μl of Precision Count beads (BioLegend) were added to the samples.

524 **Antibodies used in this study for splenocyte and BM staining**

Epitope	Conjugation	Clone	Company
CD16/CD32	NA	93	BioLegend
NK1.1	APC	PK136	BioLegend
CD19	APC	6D5	BioLegend
CD3	APC	17A2	BioLegend
Ly6G	APC	1A8	BioLegend
Ly6C	Alexa Fluor® 700™	HK1.4	BioLegend
Ly6C	Brilliant Violet 605™	HK1.4	BioLegend
CD11b	APC/Cy7	M1/70	BioLegend
CD11c	FITC	N418	BioLegend
CXCL9	PE	MIG-2F5.5	BioLegend
F4/80	PE	BM8	BioLegend
F4/80	Brilliant Violet 421™	BM8	BioLegend
I-A/I-E (MHC-II)	Brilliant Violet 605™	M5/114/15.2	BioLegend

Ly-6A/E (Sca-1)	PE/Cyanine7	E13-161.7	BioLegend
CD11c	PerCP/Cyanine5.5	N418	BioLegend
Ter-119	FITC	TER-119	BioLegend
CD4	FITC	GK1.5	BioLegend
CD8a	FITC	53-6.7	BioLegend
Gr-1	FITC	RB6-8C5	BioLegend
CD45R/B220	FITC	RA3-6B2	BioLegend
CD11b	FITC	M1/70	BioLegend
CD117/c-Kit	APC	2B8	BioLegend
Ly-6A/E (Sca-1)	PE-Vio 770™	REA422	Miltenyi

525

526 **Flow cytometry and sorting for RNA sequencing**

527 Flow cytometry and sorting was performed using the BD FACSAria III (BD). Single cells were sorted into
528 384-well plates (Eppendorf) containing 2μl of a solution containing barcoded poly-T primers for reverse
529 transcription (Sigma, Israel) according to the MARS-seq v2.0 protocol[57]. For bulk cell capture, 5-10x10^3
530 cells from each population were sorted into tubes containing 300μl RLT buffer (Qiagen) with β-
531 mercaptoethanol (BME). Immediately after sorting, plates or tubes were spun down, flash-frozen in a
532 mixture of dry ice and ethanol and stored in -80C until processing.

533 **Single-cell RNA-seq library preparation**

534 Single-cell libraries were prepared as described[57]. Briefly, mRNA from cells was converted to cDNA
535 alongside barcoding and UMI addition. The cDNA of each plate was pooled followed by second DNA
536 strand synthesis and T7 in vitro transcription. Amplified RNA was fragmented, followed by ligation of
537 partial P5 Illumina sequence, and converted to cDNA. Full sequence of barcoded P5 and P7 of P5 were
538 added by PCR for a sequence ready library. Final libraries were quantified for peak size and
539 concentration using the Agilent TapeStation and Qubit HS DNA Assay kit (Invitrogen), respectively.

540 **Bulk RNA-seq library preparation**

541 RNA was extracted and cleaned using the RNeasy mini kit (Qiagen) with DNaseI digestion. Libraries were
542 then prepared according to an in-house MARs-seq or CEL-seq protocol optimized for bulk RNA samples.

543 Final libraries were quantified for peak size and concentration using the TapeStation 4200 (Agilent) and
544 Qubit HS DNA Assay kit (Invitrogen), respectively.

545 **Library Sequencing**

546 Bulk and single cell libraries were diluted to a concentration of 1.8pM and run on the NextSeq platform
547 (Illumina) according to Illumina guidelines, with 75 reads for read1, and 15 reads for read2. A mean of
548 6M reads per library for the kinetics data; a mean of 12M reads per library for IFNγ inhibitor data; and a
549 mean of 3M reads per library for the MS4a3^{TdTm} bulk sorted population data.

550 **CD45.1/CD45.2 adoptive transfer**

551 C57BL/6J mice, expressing CD45.1 or CD45.2, were trained according to our standard protocol using BCG
552 or PBS, respectively. After two weeks, BM was isolated from the femur from both mice, resuspended in
553 PBS, and mixed in a 1:1 ratio. Recipient mice (WT C57/BL6J) were irradiated with a single dose of 950
554 cGy using an XRAD 320 machine (Precision X-Ray [PXI]) and reconstituted the next day via retro-orbital
555 injection of $5x10^6$ mixed donor BM cells/mouse in 200μl PBS. Mice were given 6 weeks to allow for
556 reconstitution and repopulation of the hematopoietic system.

557 **Flow cytometry, CFU, and spleen size analysis and quantification**

558 Flow cytometry data was analyzed using the FlowJo software.

559 For size quantification, spleens were imaged against a contrasting background, and two-dimensional
560 area was calculated using the ImageJ software.

561 All graphs quantifying the results from flow cytometry and CFU results were performed using R on
562 RStudio with the Tidyverse package[58].

563 **Bioinformatics Analysis**

564 **scRNA-seq data analysis**

565 **Data preprocessing**

566 MARS-seq pipeline[57] was used for demultiplexing, alignment to the genome (mm9), and gene counting
567 by unique molecular identifier (UMI). Overall, we sequenced 1536 cells (768 from control mouse and
568 768 from trained mouse), with 1474 median UMI count per cell and 668 median genes per cell.

569 **Data normalization and gene filtration**

570 Only genes with at least one UMI count detected in at least one cell were used. Data was normalized to
571 a library size factor. Factors were calculated by dividing total UMI counts in each cell to the median of
572 the total UMI counts across all cells. Data was transformed to log10 scale (log10(UMI count+1)). Cells
573 with less than 200 UMIs were excluded due to low coverage (24 cells, 9 from naïve mouse and 15 from
574 trained mouse). We filtered out cell cycle and ribosomal genes and selected the top 425 most variable
575 genes for further analysis. Variable genes were selected based on fitting of the data to a simple noise
576 model based on the genes mean expression and dispersion (coefficient of variance).

577 **Data clustering and annotations**

578 Principal component analysis (PCA) was performed on the variable genes, and the first 40 PCs were used
579 for downstream analysis for k-nearest neighbor (KNN)-graph, based on Euclidian distance in PC space.
580 Clustering was performed using Louvain community detection on the KNN-graph (k=20). Overall, we
581 obtained 7 clusters. Cluster identity was inferred using cluster-specific and manually selected genes
582 based on cell classification literature.

583 **Bulk RNA-seq data processing and normalization**

584 MARS-seq pipeline was used for samples demultiplexing, alignment to the genome (mm9), and gene
585 counting. Data was normalized to a library size factor. Factors were calculated by dividing the total
586 number of reads from each sample to the median total number of reads across all samples. These
587 procedures were done for each dataset alone.

588 **Kinetics data**

589 Data was transformed to log2 scale, and minimal expression threshold was set to 3. Replicate samples of
590 each condition were averaged, except for 1 sample that was excluded due to low coverage (<100k
591 reads; BCG 30d replicate 3). Preceding PCA analysis genes were centered and normalized to a mean of 0
592 and a standard deviation of 1. To identify genes that were up-regulated due to training we calculated
593 the differences between the integrals of each gene in BCG relative to PBS along time. The differences
594 across all genes were approximately normally distributed, with a mean of 0.2 and a standard deviation
595 of 10.11. Genes with more than 3 standard deviations above the mean were defined as up-regulated
596 due to training.

597 **Bulk inhibitor data**

598 Data was transformed to log2 scale, and minimal expression threshold was set to 3. Two Fedratinib
599 samples were excluded from analysis due to technical issues during injection that resulted in a lack of
600 inhibition. Heatmap was generated using DEGs calculated by ANOVA (5% FDR and a minimal 2-fold; 167
601 genes).

602 **Fedratinib inhibitor data**

603 Data was transformed to log2 scale, and minimal expression threshold was set to 4. One sample was
604 excluded due to low coverage (<100k reads; PBS +S.*Tm* + Fedratinib replicate 3). Preceding PCA analysis
605 genes were centered and normalized to a mean of 0 and a standard deviation of 1. PCA analysis was
606 performed on DEGs calculated using two-sided t-tests between all relevant conditions: control vs.
607 trained samples, trained with or without inhibitor, control with or without inhibitor, uninfected vs.
608 infected, infected with or without training, infected vs. infected with training with inhibitor, and infected
609 with training vs. infected with training with inhibitor (5% FDR; 453 genes). Heatmap was generated using
610 two-sample t-test between control and BCG-trained samples (1% FDR).

611 **αIFNγ inhibitor data**

612 Data was transformed to log2 scale, and minimal expression threshold was set to 3. Two sample was
613 excluded due to low coverage (<250k reads CM BCG + Isotype replicate 1 and RPM BCG + Isotype
614 replicate 4). Heatmap genes were selected from cluster I and II from the lineage tracing experiment
615 representing shared interferon/STAT-1 upregulated genes.

616 **MS4A3^{Tdtm} bulk population data**

617 Data was transformed to log2 scale, and minimal expression threshold was set to 3. One sample was
618 excluded due to low coverage (<150k reads; control NCM-Tdtm^{+} replicate 4). Preceding PCA analysis
619 genes were centered and normalized to a mean of 0 and a standard deviation of 1. DEGs between
620 control and trained mice were calculated using two-sided t-test between all control samples versus all
621 trained samples (from all sorted populations together; 10% FDR, 382 genes).

622

623

Acknowledgments

This research was supported by the Israel Science Foundation (ISF grant No. 1289/22), the Minerva Foundation with funding from the Federal Ministry for Education and Research, the Dr. Barry Sherman Institute for Medicinal Chemistry, and the Shimon and Golde Picker Weizmann Annual Grant.

Author contributions

AS and RA designed the study. AS, DH, ST and LV performed the experiments. DY and NBBM analyzed the data. AS and RA wrote the manuscript.

Competing Interests

The authors declare no competing interests

Data and materials availability

All RNA-seq data have been deposited in NCBI's Gene Expression Omnibus (GEO) under the super-series accession number GSE252014.

637 ## References

638

639 1. Arts, R. J. W. *et al.* Long-term in vitro and in vivo effects of γ-irradiated BCG on innate and adaptive
640 immunity. *Journal of Leukocyte Biology* **98**, 995–1001 (2015).
641 2. Saeed, S. *et al.* Epigenetic programming of monocyte-to-macrophage differentiation and trained
642 innate immunity. *Science* **345**, 1251086 (2014).
643 3. Darrah, P. A. *et al.* Prevention of tuberculosis in macaques after intravenous BCG immunization.
644 *Nature* **577**, 95–102 (2020).
645 4. Moorlag, S. J. C. F. M., Arts, R. J. W., van Crevel, R. & Netea, M. G. Non-specific effects of BCG
646 vaccine on viral infections. *Clinical Microbiology and Infection* **25**, 1473–1478 (2019).
647 5. Hasso-Agopsowicz, M. *et al.* Identifying WHO global priority endemic pathogens for vaccine
648 research and development (R&D) using multi-criteria decision analysis (MCDA): an objective of the
649 Immunization Agenda 2030. *eBioMedicine* **0**, (2024).
650 6. Qadri, F. *et al.* 5-year vaccine protection following a single dose of Vi-tetanus toxoid conjugate
651 vaccine in Bangladeshi children (TyVOID): a cluster randomised trial. *The Lancet* **404**, 1419–1429
652 (2024).
653 7. Kurotaki, D., Uede, T. & Tamura, T. Functions and development of red pulp macrophages.
654 *Microbiology and Immunology* **59**, 55–62 (2015).
655 8. Hoeffel, G. *et al.* C-Myb(+) erythro-myeloid progenitor-derived fetal monocytes give rise to adult
656 tissue-resident macrophages. *Immunity* **42**, 665–678 (2015).
657 9. Lai, S. M. *et al.* Organ-Specific Fate, Recruitment, and Refilling Dynamics of Tissue-Resident
658 Macrophages during Blood-Stage Malaria. *Cell Reports* **25**, 3099-3109.e3 (2018).
659 10. Zhang, L. *et al.* Variable Virulence and Efficacy of BCG Vaccine Strains in Mice and Correlation With
660 Genome Polymorphisms. *Molecular Therapy* **24**, 398–405 (2016).
661 11. Review of the macrophage disappearance reaction - Barth - 1995 - Journal of Leukocyte Biology -
662 Wiley Online Library. https://jlb.onlinelibrary.wiley.com/doi/abs/10.1002/jlb.57.3.361.
663 12. Keren-Shaul, H. *et al.* MARS-seq2.0: an experimental and analytical pipeline for indexed sorting
664 combined with single-cell RNA sequencing. *Nat Protoc* **14**, 1841–1862 (2019).
665 13. Hu, X. & Ivashkiv, L. B. Cross-regulation of Signaling and Immune Responses by IFN-γ and STAT1.
666 *Immunity* **31**, 539–550 (2009).
667 14. Kaufmann, E. *et al.* BCG Educates Hematopoietic Stem Cells to Generate Protective Innate Immunity
668 against Tuberculosis. *Cell* **172**, 176-190.e19 (2018).
669 15. Yang, S.-H. *et al.* IFN-γ–STAT1–iNOS Induces Myeloid Progenitors to Acquire Immunosuppressive
670 Activity. *Frontiers in Immunology* **8**, (2017).
671 16. Biram, A. *et al.* Bacterial infection disrupts established germinal center reactions through monocyte
672 recruitment and impaired metabolic adaptation. *Immunity* **55**, 442-458.e8 (2022).
673 17. Penton-Rol, G. *et al.* Selective Inhibition of Expression of the Chemokine Receptor CCR2 in Human
674 Monocytes by IFN-γ1. *The Journal of Immunology* **160**, 3869–3873 (1998).
675 18. Wang, Y. *et al.* Bacillus Calmette–Guérin–induced interleukin-10 inhibits S100A8/A9 production and
676 hinders development of T helper type 1 memory in mice. *European Journal of Immunology* **53**,
677 2250204 (2023).
678 19. Liu, K. *et al.* Neutrophilic granule protein (NGP) attenuates lipopolysaccharide-induced
679 inflammatory responses and enhances phagocytosis of bacteria by macrophages. *Cytokine* **128**,
680 155001 (2020).
681 20. Khan, N. *et al.* M. tuberculosis Reprograms Hematopoietic Stem Cells to Limit Myelopoiesis and
682 Impair Trained Immunity. *Cell* **183**, 752-770.e22 (2020).

683 21. Hoffman, D. *et al.* A non-classical monocyte-derived macrophage subset provides a splenic
684 replication niche for intracellular Salmonella. *Immunity* **54**, 2712-2723.e6 (2021).
685 22. Yona, S. *et al.* Fate mapping reveals origins and dynamics of monocytes and tissue macrophages
686 under homeostasis. *Immunity* **38**, 79–91 (2013).
687 23. Tretina, K., Park, E.-S., Maminska, A. & MacMicking, J. D. Interferon-induced guanylate-binding
688 proteins: Guardians of host defense in health and disease. *J Exp Med* **216**, 482–500 (2019).
689 24. Clement, M. *et al.* IFITM3 restricts virus-induced inflammatory cytokine production by limiting
690 Nogo-B mediated TLR responses. *Nat Commun* **13**, 5294 (2022).
691 25. Carow, B. *et al.* Critical and independent role for SOCS3 in either myeloid or T cells in resistance to
692 Mycobacterium tuberculosis. *PLoS Pathog* **9**, e1003442 (2013).
693 26. Bomfim, C. C. B. *et al.* Mycobacterium tuberculosis Induces Irg1 in Murine Macrophages by a
694 Pathway Involving Both TLR-2 and STING/IFNAR Signaling and Requiring Bacterial Phagocytosis.
695 *Front Cell Infect Microbiol* **12**, 862582 (2022).
696 27. Vogt, A.-C. S. *et al.* On Iron Metabolism and Its Regulation. *International Journal of Molecular*
697 *Sciences* **22**, 4591 (2021).
698 28. Liu, Z. *et al.* Fate Mapping via Ms4a3-Expression History Traces Monocyte-Derived Cells. *Cell* **178**,
699 1509-1525.e19 (2019).
700 29. Yáñez, A. *et al.* Granulocyte-Monocyte Progenitors and Monocyte-Dendritic Cell Progenitors
701 Independently Produce Functionally Distinct Monocytes. *Immunity* **47**, 890-902.e4 (2017).
702 30. De Leon-Oliva, D. *et al.* AIF1: Function and Connection with Inflammatory Diseases. *Biology (Basel)*
703 **12**, 694 (2023).
704 31. Prevete, N., Liotti, F., Marone, G., Melillo, R. M. & de Paulis, A. Formyl peptide receptors at the
705 interface of inflammation, angiogenesis and tumor growth. *Pharmacol Res* **102**, 184–191 (2015).
706 32. Gibbings, D. J., Marcet-Palacios, M., Sekar, Y., Ng, M. C. Y. & Befus, A. D. CD8 alpha is expressed by
707 human monocytes and enhances Fc gamma R-dependent responses. *BMC Immunol* **8**, 12 (2007).
708 33. Sugimoto, M. A., Vago, J. P., Teixeira, M. M. & Sousa, L. P. Annexin A1 and the Resolution of
709 Inflammation: Modulation of Neutrophil Recruitment, Apoptosis, and Clearance. *J Immunol Res*
710 **2016**, 8239258 (2016).
711 34. Håversen, L. *et al.* Vimentin deficiency in macrophages induces increased oxidative stress and
712 vascular inflammation but attenuates atherosclerosis in mice. *Sci Rep* **8**, 16973 (2018).
713 35. Karlstetter, M. *et al.* The Novel Activated Microglia/Macrophage WAP Domain Protein, AMWAP,
714 Acts as a Counter-Regulator of Proinflammatory Response. *The Journal of Immunology* **185**, 3379–
715 3390 (2010).
716 36. Kernbauer, E. *et al.* Conditional Stat1 Ablation Reveals the Importance of Interferon Signaling for
717 Immunity to Listeria monocytogenes Infection. *PLoS Pathog* **8**, e1002763 (2012).
718 37. Lé, A. M., Puig, L. & Torres, T. Deucravacitinib for the Treatment of Psoriatic Disease. *Am J Clin*
719 *Dermatol* **23**, 813–822 (2022).
720 38. Kalafati, L. *et al.* Innate Immune Training of Granulopoiesis Promotes Anti-tumor Activity. *Cell* **183**,
721 771-785.e12 (2020).
722 39. Huijser, E. *et al.* Trained Immunity in Primary Sjögren's Syndrome: Linking Type I Interferons to a
723 Pro-Atherogenic Phenotype. *Frontiers in Immunology* **13**, (2022).
724 40. Zahalka, S. *et al.* Trained immunity of alveolar macrophages requires metabolic rewiring and type 1
725 interferon signaling. *Mucosal Immunol* **15**, 896–907 (2022).
726 41. Moorlag, S. J. C. F. M. *et al.* β-Glucan Induces Protective Trained Immunity against Mycobacterium
727 tuberculosis Infection: A Key Role for IL-1. *Cell Reports* **31**, 107634 (2020).
728 42. Li, X. *et al.* GBP2 promotes M1 macrophage polarization by activating the notch1 signaling pathway
729 in diabetic nephropathy. *Front. Immunol.* **14**, (2023).

730 43. Meunier, E. *et al.* Caspase-11 activation requires lysis of pathogen-containing vacuoles by IFN-
731 induced GTPases. *Nature* **509**, 366–370 (2014).
732 44. Groom, J. R. & Luster, A. D. CXCR3 ligands: redundant, collaborative and antagonistic functions.
733 *Immunol Cell Biol* **89**, 207–215 (2011).
734 45. Joosten, S. A. *et al.* Mycobacterial growth inhibition is associated with trained innate immunity. *The*
735 *Journal of Clinical Investigation* **128**, 1837 (2018).
736 46. Lampropoulou, V. *et al.* Itaconate Links Inhibition of Succinate Dehydrogenase with Macrophage
737 Metabolic Remodeling and Regulation of Inflammation. *Cell Metab* **24**, 158–166 (2016).
738 47. Michelucci, A. *et al.* Immune-responsive gene 1 protein links metabolism to immunity by catalyzing
739 itaconic acid production. *Proc Natl Acad Sci U S A* **110**, 7820–7825 (2013).
740 48. Domínguez-Andrés, J. *et al.* The Itaconate Pathway Is a Central Regulatory Node Linking Innate
741 Immune Tolerance and Trained Immunity. *Cell Metabolism* **29**, 211-220.e5 (2019).
742 49. Liao, C., Prabhu, K. S. & Paulson, R. F. Monocyte-derived macrophages expand the murine stress
743 erythropoietic niche during the recovery from anemia. *Blood* **132**, 2580–2593 (2018).
744 50. Haldar, M. *et al.* Heme-mediated SPI-C induction promotes monocyte differentiation into iron-
745 recycling macrophages. *Cell* **156**, 1223–1234 (2014).
746 51. Akter, S. *et al.* Mycobacterium tuberculosis infection drives a type I IFN signature in lung
747 lymphocytes. *Cell Reports* **39**, 110983 (2022).
748 52. Shmerling, M. *et al.* LY6S, a New IFN-Inducible Human Member of the Ly6a Subfamily Expressed by
749 Spleen Cells and Associated with Inflammation and Viral Resistance. *ImmunoHorizons* **6**, 253–272
750 (2022).
751 53. Vierboom, M. P. M. *et al.* Stronger induction of trained immunity by mucosal BCG or MTBVAC
752 vaccination compared to standard intradermal vaccination. *Cell Rep Med* **2**, 100185 (2021).
753 54. Jeyanathan, M. *et al.* Parenteral BCG vaccine induces lung-resident memory macrophages and
754 trained immunity via the gut–lung axis. *Nat Immunol* **23**, 1687–1702 (2022).
755 55. Thomas, G. D. *et al.* Deleting an Nr4a1 Super-Enhancer Subdomain Ablates Ly6Clow Monocytes
756 while Preserving Macrophage Gene Function. *Immunity* **45**, 975–987 (2016).
757 56. Stapels, D. A. C. *et al.* Salmonella persisters undermine host immune defenses during antibiotic
758 treatment. *Science* **362**, 1156–1160 (2018).
759 57. MARS-seq2.0: an experimental and analytical pipeline for indexed sorting combined with single-cell
760 RNA sequencing | Nature Protocols. https://www.nature.com/articles/s41596-019-0164-4.
761 58. Wickham, H. *et al.* Welcome to the Tidyverse. *Journal of Open Source Software* **4**, 1686 (2019).
762

763

764 ## Figure legends

765

766 **Figure 1. Intraperitoneal BCG results in heterologous *S*.Tm protection and a distinct myeloid subsets**
767 **with signatures driven by STAT1.** (**A) Mouse model of BCG vaccination and S.Tm challenge**. (**B**) Splenic
768 S.*Tm* CFU 24 hours post infection between control (n=11) and trained mice (n=11). (**C-D**) Flow cytometry
769 plots of myeloid populations two weeks post vaccination (C) and mean percentage fold change of BCG
770 over control for each given gated population percent from the Lin^- population (D). (**E**) K-nearest
771 neighbors (KNN) plot for total $CD11b^+$ single cells sorted from control and BCG mice. Color is based on
772 conditions, or cluster identity. (**F**) Cell markers and training induced genes for each subset. Size and color
773 intensity indicates percentage of cells within a given cluster expressing the gene and average expression.
774 (**G**) Proportions of monocyte subsets based on classifications in E. (**H-I**) Number of DEGs in each cell
775 subset (H), and their corresponding gene set enrichment analysis (I). (**J**) Volcano plot of DEGs in CM
776 subset. Data in bar graphs are presented as mean±SEM, with each individual point in **B** a biological
777 repeat. Two-tailed *t*-test used for data in **B** and **D** (**P*<0.05, ***P*<0.01).

778

779 **Figure 2. Dynamics of TI-associated subsets and signatures indicates early and delayed kinetics.** (**A**)
780 Experimental setup tracking TI kinetics over a two-month interval, including S.Tm challenge at days 14
781 and 60. (**B**) Splenic *S.Tm* CFU at 24 hours post infection for control and BCG mice at 14- and 60- days
782 after vaccination (n=5-6). (**C**) BCG CFU from spleen and BM of BCG vaccinated mice (n=4) across time
783 points. Red-dotted line indicates limit of detection. (**D**) Contribution of MP populations across time
784 points from control (PBS) and BCG mice (days post injection). Percentage of CM, NCM, and dendritic
785 cells calculated from flow cytometry analysis of $CD11b^+$ population. Percentage of RPM calculated from
786 Lin^- population (control: n=3, BCG: n=4 in each time point). PBS values are the mean of all time points.
787 (**E**) Heatmap of upregulated genes due to training and relative gene expression ordered according to
788 peak expression time. (**F**) Gene set enrichment analysis of DEGs in days 14 and 30. (**G-H**) Heatmap of
789 IFNγ response genes (G) and their average expression dynamics compared to STAT1 expression (H). Data
790 in bar and line graphs are presented as mean±SEM. For bar graph **B** and **C**, each individual point is a
791 biological repeat. For line graph **H**, significance represents comparison between day 60 control and BCG.
792 Heatmap rows in **E** and **G** indicate biological replicates. Two-tailed *t*-test used for data in **B**, **C**, and **H**
793 **(****P*<0.05, ***P*<0.01, ****P*<0.005, *****P*<0.001**)**.

794 **Figure 3. RPM niche is replenished by recruited trained monocytes and by local training of tissue-**
795 **resident populations**. (**A**) Scheme representing known myeloid differentiation pathways and potential
796 trans-differentiation of trained CM to RPM. (**B**) Mouse model to track contribution of TI-associated
797 signatures in local and recruited MP populations with lineage tracing. (**C-D**) Flow cytometry analysis of
798 $TdTm^+$ or $Tdtm^-$ $Ly6C^+$ MPs and RPM and quantification of RPM $TdTm^+$ subset (n=3). (**D-F**) Number of
799 DEGs of each sorted population (D), heatmap of normalized log2 expression from TI-associated DEGs
800 specific to trained RPM populations and gene set enrichment analysis of DEGs in each sorted population
801 (F). Data in bar graphs are presented as mean±SEM. Heatmap rows in **E** indicate biological replicates.
802 Two-tailed *t*-test used for data in **C** (**P*<0.05).

803

804 **Figure 4. Transient IFNγ-STAT1 inhibition prevents TI signatures and splenic infection resistance.** (**A**)
805 Mouse model of BCG vaccination with early interferon inhibition using the Fedratinib inhibitor. (**B**)
806 Splenic S.*Tm* CFU for control and BCG mice, with and without Fedratinib inhibitor, 24h post infection
807 (n=2-6).(**C**) MP populations from control (gray) and BCG (black) mice, with or without Fedratinib
808 inhibition. Percentage of CM and NCM cells calculated from $CD11b^+$ population. Percentage of RPM
809 calculated from Lin^- population. (**D**) Percentage of $CXCL9^+$ CM-T, NCM, and RPM populations from
810 control (gray) and BCG (black) mice, with or without Fedratinib inhibition (control: n=3, BCG: n=4,
811 control+Fedratinib: n=3, BCG+Fedratinib: n=6). (**E**) Heatmap of normalized log2 expression of DEGs
812 across naïve and training conditions. (**F**) Gene set enrichment analysis of DEGs from E. Data in bar graphs
813 are presented as mean±SEM. For bar graph **B** each individual point is a biological repeat. Heatmap rows
814 in E indicate biological replicates. Two-tailed *t*-test used for data in **B**, **C**, and **D** (**P*<0.05, ***P*<0.01,
815 ****P*<0.005, *****P*<0.001**)**.

816

Figure 1

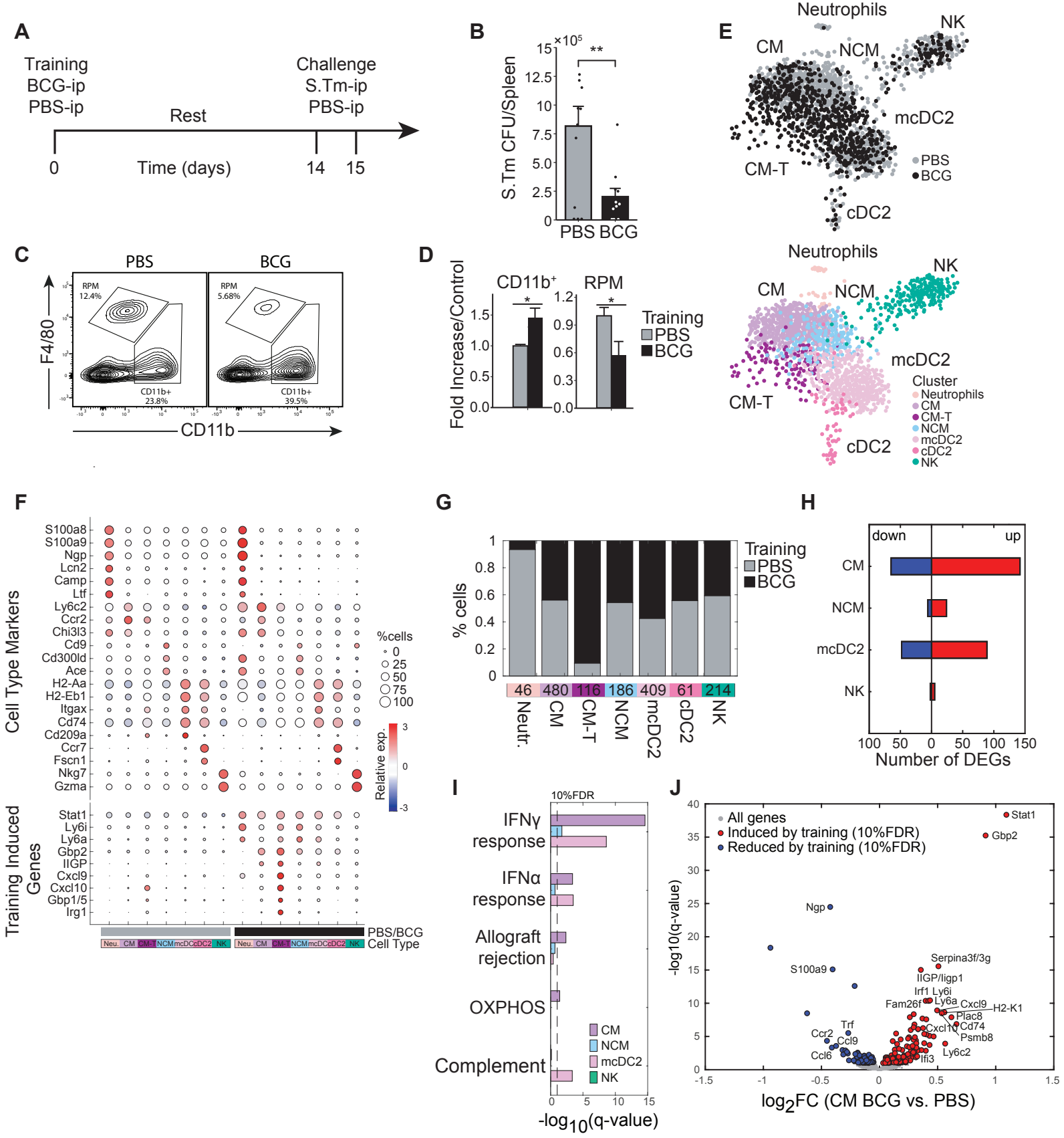
A
Training
BCG-ip
PBS-ip
Rest
Challenge
S.Tm-ip
PBS-ip
0
Time (days)
14
15
B
S.Tm CFU/Spleen
×10^5
**
PBS
BCG
C
PBS
BCG
RPM
12.4%
RPM
5.68%
CD11b+
23.8%
CD11b+
39.5%
F4/80
CD11b
D
CD11b+
RPM
Fold Increase/Control
Training
PBS
BCG
E
Neutrophils
NK
CM
NCM
mcDC2
CM-T
cDC2
PBS
BCG
Cluster
Neutrophils
CM
CM-T
NCM
mcDC2
cDC2
NK
F
Cell Type Markers
S100a8
S100a9
Ngp
Lcn2
Camp
Ltf
Ly6c2
Ccr2
Chi3l3
Cd9
Cd300ld
Ace
H2-Aa
H2-Eb1
Itgax
Cd74
Cd209a
Ccr7
Fscn1
Nkg7
Gzma
Training Induced Genes
Stat1
Ly6i
Ly6a
Gbp2
IIGP
Cxcl9
Cxcl10
Gbp1/5
Irg1
%cells
0
25
50
75
100
Relative exp.
3
0
-3
PBS/BCG
Cell Type
Neu.
CM
CM-T
NCM
mcDC
cDC2
NK
G
% cells
Training
PBS
BCG
46
480
116
186
409
61
214
Neutr.
CM
CM-T
NCM
mcDC2
cDC2
NK
H
down
up
CM
NCM
mcDC2
NK
Number of DEGs
I
10%FDR
IFNγ response
IFNα response
Allograft rejection
OXPHOS
Complement
CM
NCM
mcDC2
NK
-log10(q-value)
J
All genes
Induced by training (10%FDR)
Reduced by training (10%FDR)
Stat1
Gbp2
Ngp
S100a9
Serpina3f/3g
IIGP/Iigp1
Irf1
Ly6i
Fam26f
Ly6a
Cxcl9
H2-K1
Plac8
Cxcl10
Cd74
Psmb8
Ly6c2
Ifi3
Trf
Ccr2
Ccl9
Ccl6
-log10(q-value)
log2FC (CM BCG vs. PBS)

Figure 2

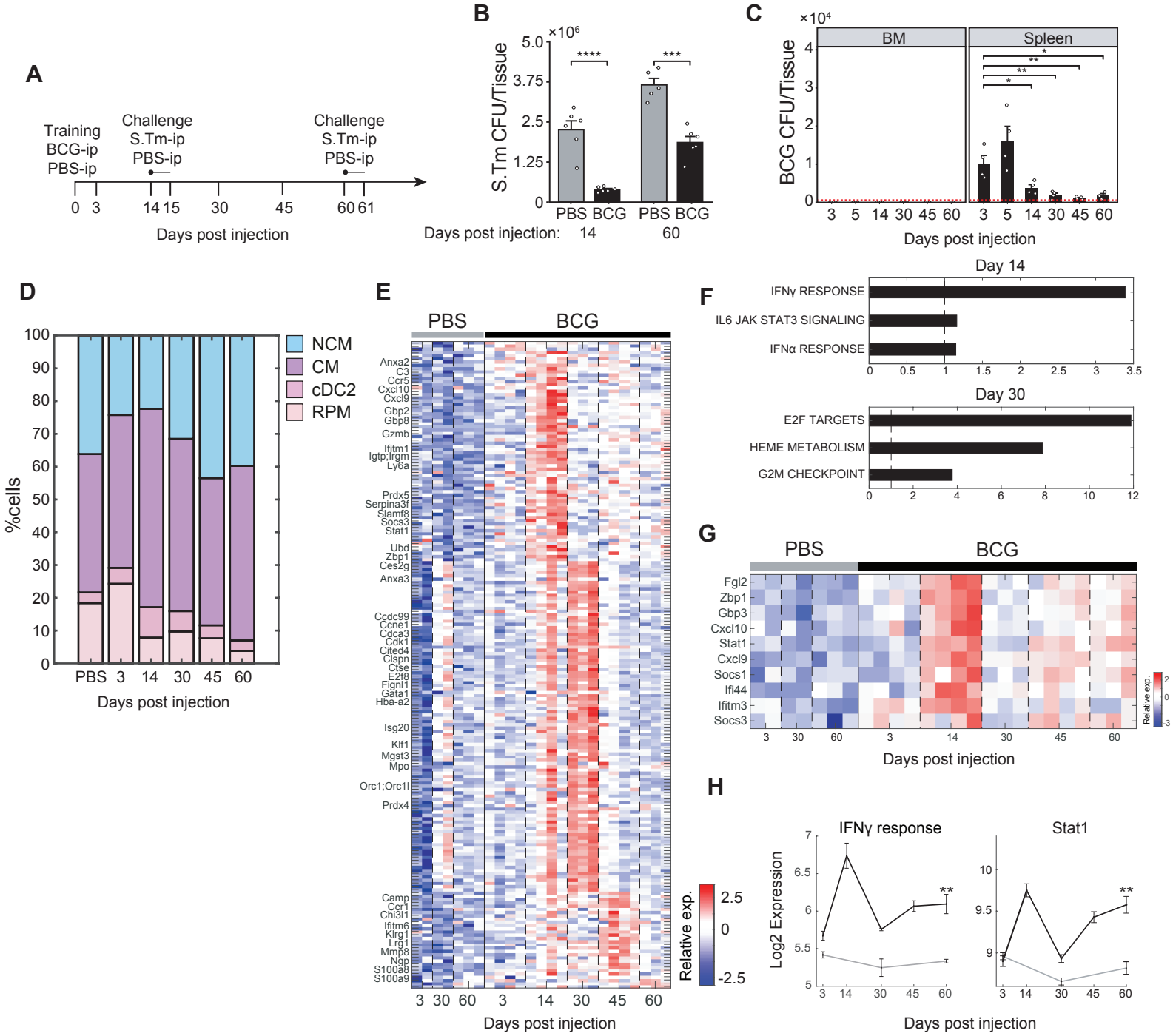
A
Training
BCG-ip
PBS-ip
Challenge
S.Tm-ip
PBS-ip
Challenge
S.Tm-ip
PBS-ip
0 3 14 15 30 45 60 61
Days post injection
B
S.Tm CFU/Tissue
×10^6
5.0
3.75
2.5
1.25
0
****
***
PBS BCG PBS BCG
Days post injection: 14 60
C
BCG CFU/Tissue
×10^4
BM
Spleen
3 5 14 30 45 60 3 5 14 30 45 60
Days post injection
D
%cells
NCM
CM
cDC2
RPM
PBS 3 14 30 45 60
Days post injection
E
PBS
BCG
Anxa2
C3
Ccr5
Cxcl10
Cxcl9
Gbp2
Gbp8
Gzmb
Ifitm1
Igtp;Irgm
Ly6a
Prdx5
Serpina3f
Slamf8
Socs3
Stat1
Ubd
Zbp1
Ces2g
Anxa3
Ccdc99
Ccne1
Cdca3
Cdk1
Cited4
Clspn
Ctse
E2f8
Fign1
Gata1
Hba-a2
Isg20
Klf1
Mgst3
Mpo
Orc1;Orc1l
Prdx4
Camp
Ccr1
Chil3l1
Ifitm6
Klrg1
Lrg1
Mmp8
Ngp
S100a8
S100a9
3 30 60 3 14 30 45 60
Days post injection
Relative exp.
2.5
0
-2.5
F
Day 14
IFNγ RESPONSE
IL6 JAK STAT3 SIGNALING
IFNα RESPONSE
Day 30
E2F TARGETS
HEME METABOLISM
G2M CHECKPOINT
G
PBS
BCG
Fgl2
Zbp1
Gbp3
Cxcl10
Stat1
Cxcl9
Socs1
Ifi44
Ifitm3
Socs3
3 30 60 3 14 30 45 60
Days post injection
Relative exp.
H
IFNγ response
Stat1
Log2 Expression
Days post injection

Figure 3

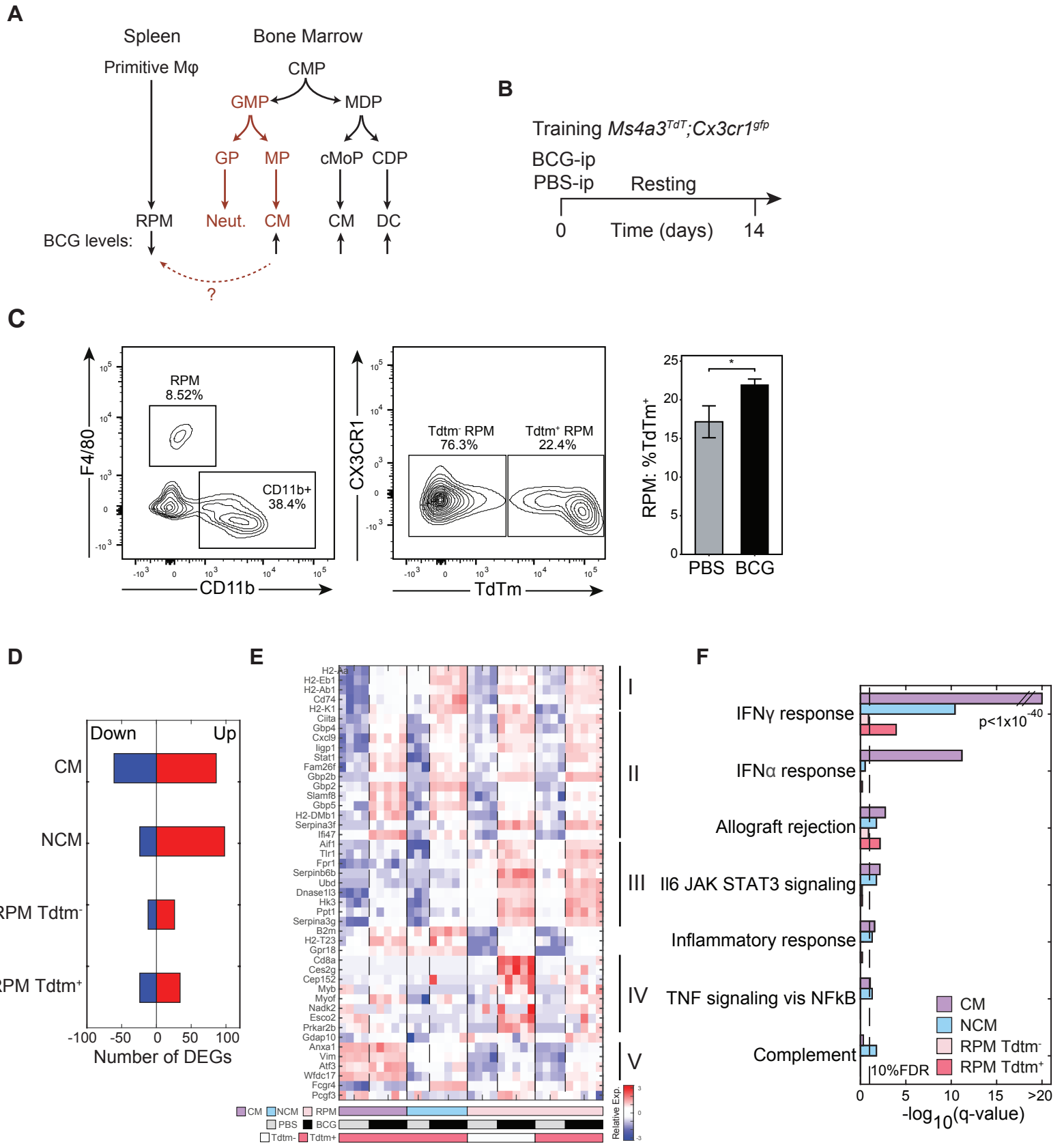
A
Spleen
Bone Marrow
Primitive Mφ
CMP
GMP
MDP
GP
MP
cMoP
CDP
RPM
Neut.
CM
CM
DC
BCG levels:
?
B
Training Ms4a3TdT;Cx3cr1gfp
BCG-ip
PBS-ip
Resting
0
Time (days)
14
C
RPM
8.52%
CD11b+
38.4%
F4/80
CD11b
Tdtm- RPM
76.3%
Tdtm+ RPM
22.4%
CX3CR1
TdTm
RPM: %TdTm+
PBS
BCG
D
Down
Up
CM
NCM
RPM Tdtm-
RPM Tdtm+
Number of DEGs
E
I
II
III
IV
V
Relative Exp.
CM
NCM
RPM
PBS
BCG
Tdtm-
Tdtm+
F
IFNγ response
IFNα response
Allograft rejection
Il6 JAK STAT3 signaling
Inflammatory response
TNF signaling vis NFkB
Complement
p<1x10-40
10%FDR
CM
NCM
RPM Tdtm-
RPM Tdtm+
-log10(q-value)

Figure 4

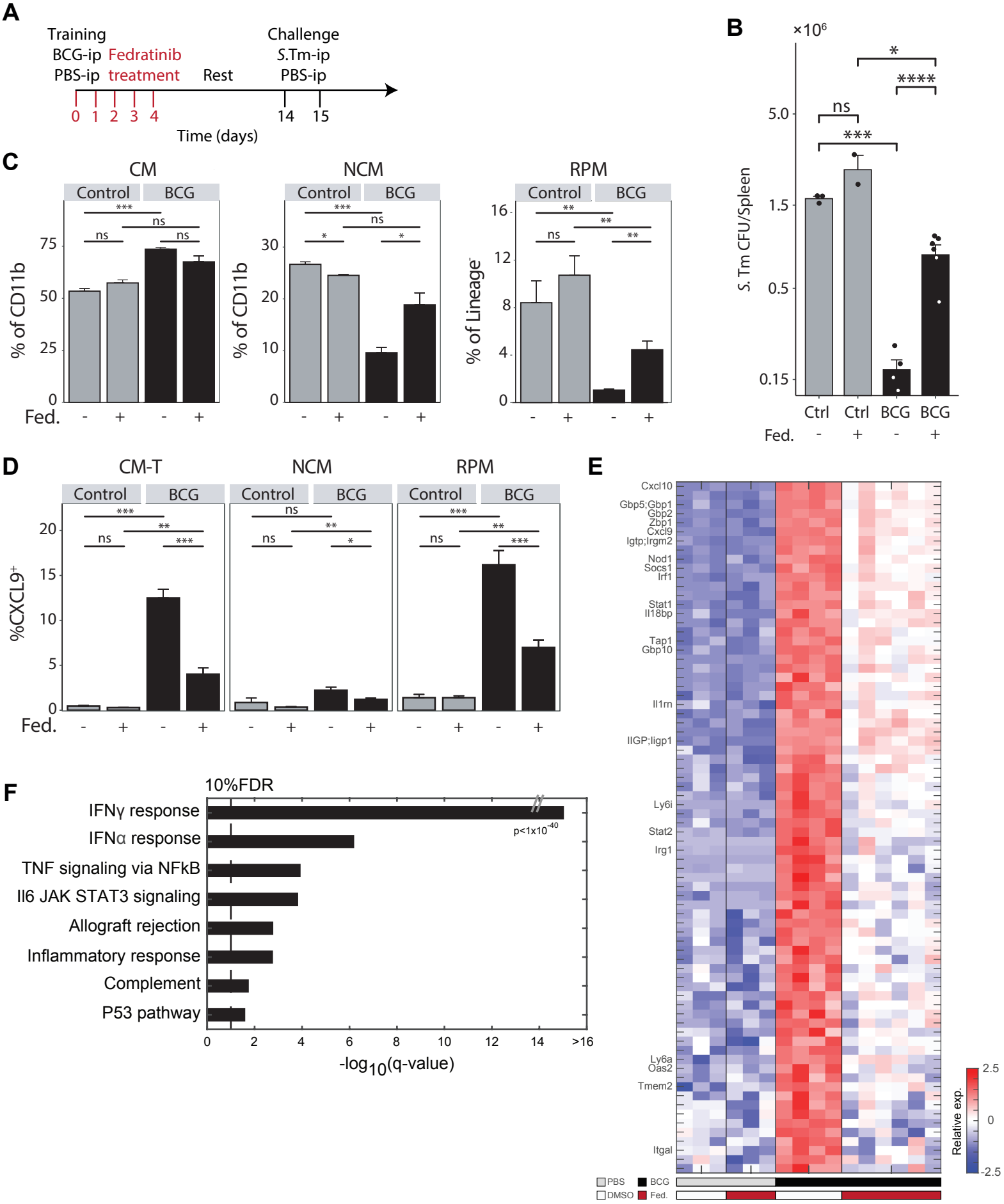
A
Training
BCG-ip
PBS-ip
Fedratinib
treatment
Rest
Challenge
S.Tm-ip
PBS-ip
0 1 2 3 4
14 15
Time (days)
B
×10^6
S. Tm CFU/Spleen
Ctrl Ctrl BCG BCG
Fed. - + - +
C
CM
NCM
RPM
Control
BCG
% of CD11b
% of Lineage
Fed. - + - +
D
CM-T
NCM
RPM
%CXCL9+
Fed. - + - + - + - + - + - +
E
Cxcl10
Gbp5;Gbp1
Gbp2
Zbp1
Cxcl9
Igtp;Irgm2
Nod1
Socs1
Irf1
Stat1
Il18bp
Tap1
Gbp10
Il1rn
IIGP;Iigp1
Ly6i
Stat2
Irg1
Ly6a
Oas2
Tmem2
Itgal
Relative exp.
PBS
DMSO
BCG
Fed.
F
10%FDR
IFNγ response
IFNα response
TNF signaling via NFkB
Il6 JAK STAT3 signaling
Allograft rejection
Inflammatory response
Complement
P53 pathway
p<1x10^-40
-log10(q-value)